Kinetics of the reactions of nitrogen dioxide with CH3S, CH3SO, CH3SS, and CH3SSO at 297 K and 1 torr

ARTICLE *in* THE JOURNAL OF PHYSICAL CHEMISTRY · JULY 1990

Impact Factor: 2.78 · DOI: 10.1021/j100378a043

3 AUTHORS, INCLUDING:

Florent Domine
Laval University
155 PUBLICATIONS **3,965** CITATIONS

Schrödinger equation with the solvent polarization dependent wave function, and vice versa.[10,11] The dynamical aspects of this problem of CS in strongly interacting D-A systems are now becoming a subject of lively investigations from both experimental and theoretical viewpoints.[5,12-14] It seems that such a mechanism has not been taken into account explicitly in the conventional electron-transfer theories. Nevertheless, it may be important in the actual photoinduced CS reactions in solution and, probably, also in amorphous solids, when D, A pairs undergo the electron transfer due to the relatively strong electronic interaction.

The IP state formed by the CS in the course of the relaxation including the structural rearrangement from the Franck-Condon excited state of the TCNB complexes undergoes charge recombination decay and, in strongly polar solvents, dissociation into free ions. The investigations on the dynamics and mechanisms of these processes will be discussed in a forthcoming paper.

Acknowledgment. N.M. acknowledges the support by Grant-in-Aid (No. 62065006) from the Ministry of Education, Science and Culture, Japan.

(9) Mataga, N.; Kubota, T. *Molecular Interactions and Electronic Spectra*; Marcel Dekker: New York, 1970; pp 448-458.
(10) (a) Beens, H.; Weller, A. *Chem. Phys. Lett.* **1969**, *3*, 666. (b) In *Organic Molecular Photophysics*; Birks, J. B., Ed.; Wiley-Interscience: London, 1975; Vol. 2, pp 159-215.
(11) (a) Mataga, N. In *The Exciplex*; Gordon, M., Ware, W. R., Eds.; Academic: New York, 1975; pp 113-144. (b) In *Molecular Interactions*; Ratajczak, H., Orville-Thomas, W. J., Eds.; Wiley: New York, 1981; Vol. 2, pp 509-570.
(12) Mataga, N.; Yao, H.; Okada, T.; Rettig, W. *J. Phys. Chem.* **1989**, *93*, 3383.
(13) Barbara, P. F.; Kang, T. J.; Jarzeba, W.; Fonseca, T. In *Perspectives in Photosynthesis*; Jortner, J., Pullman, B., Eds.; Kluwer-Academic: Dordrecht, 1990; pp 273-292.
(14) Kim, H. J.; Hynes, J. T. *J. Phys. Chem.* **1990**, *94*, 2736.

Kinetics of the Reactions of NO_2 with CH_3S, CH_3SO, CH_3SS, and CH_3SSO at 297 K and 1 Torr

Florent Dominé, Timothy P. Murrells, and Carleton J. Howard*

National Oceanic and Atmospheric Administration, ERL, R/E/AL2, 325 Broadway, Boulder, Colorado 80303, and the Cooperative Institute for Research in Environmental Sciences, University of Colorado, Boulder, Colorado *(Received: November 20, 1989; In Final Form: March 7, 1990)*

The rate constants for the reactions of NO_2 with CH_3S (1), CH_3SO (2), CH_3SS (3), and CH_3SSO (4) have been measured at 297 K and 1 Torr in a discharge flow tube with photoionization mass spectrometric detection. The detection limits of the sulfur radicals studied were in the 10^6 molecules cm^{-3} range. The rate constant values obtained are (in cm^3 $molecule^{-1}$ s^{-1}) $k_1 = (5.1 \pm 0.9) \times 10^{-11}$, $k_2 = (1.2 \pm 0.25) \times 10^{-11}$, $k_3 = (1.8 \pm 0.3) \times 10^{-11}$, and $k_4 = (4.5 \pm 1.2) \times 10^{-12}$. The yield of CH_3SO in reaction 1 has been found to be unity. Curvature observed on some of the decay plots was attributed to the fragmentation of ions in the ionization chamber.

Introduction

The knowledge of the oxidation mechanism of the naturally emitted reduced sulfur compounds has been considered essential to understand background acid precipitation. Recently, Charlson et al.[1] have suggested that dimethyl sulfide (DMS), which accounts for about half of the natural sulfur emissions[2-4] and is emitted mainly by phytoplankton, could be oxidized to form aerosols, which would have a negative feedback on the tropospheric warming due to the greenhouse effect. This suggestion is still controversial[5-11] but certainly adds some interest to the investigation of the oxidation pathways of DMS and of the other reduced sulfur compounds.

The radicals presently thought to be involved in the initiation of the atmospheric oxidation of DMS are OH, NO_3, and IO. The oxidation of DMS by IO gives $CH_3S(O)CH_3$ (DMSO)[12,13] and could be the major sink of DMS in the coastal regions, where large amounts of IO are present.[14] The oxidation of DMS by NO_3 has been investigated by several groups,[15-19] but the intermediates produced by this reaction are not known, although Dlugokencky and Howard[19] suggest that CH_3S is not formed in that reaction. A large amount of indirect evidence[20-22] suggests that CH_3S is formed in the OH-initiated oxidation of DMS. The proposed reactions leading to CH_3S are

$$CH_3SCH_3 + OH \rightarrow CH_3SCH_2 + H_2O$$

$$CH_3SCH_2 + O_2 \xrightarrow{M} CH_3SCH_2OO$$

$$CH_3SCH_2OO + NO \rightarrow CH_3SCH_2O + NO_2$$

$$CH_3SCH_2O \rightarrow CH_3S + CH_2O$$

Thus it appears that CH_3S could be a major intermediate in the oxidation of DMS, especially in areas where the amount of NO_3

* Author to whom correspondence should be addressed at NOAA.

(1) Charlson, R. J.; Lovelock, J. E.; Andreae, M. O.; Warren, S. G. *Nature* **1987**, *326*, 655.
(2) Andreae, M. O. In *The Biogeochemical Cycling of Sulfur and Nitrogen in the Remote Atmosphere*; Galloway, J. N., et al., Eds.; D. Reidel: Dordrecht: 1985; pp 5-25.
(3) Andreae, M. O.; Ferek, R. J.; Bermond, F.; Byrd, K. P.; Engstron, R. T.; Hardin, S.; Houmere, P. D.; Le Marrec, F.; Raemdonck, H.; Chatfield, R. B. *J. Geophys. Res.* **1986**, *D90*, 12891.
(4) Toon, O. T.; Kastings, J. F.; Turco, R. P.; Liu, M. S. *J. Geophys. Res.* **1987**, *92*, 943.
(5) Schwartz, S. E. *Nature* **1988**, *336*, 441.
(6) Caldeira, K. *Nature* **1989**, *337*, 732.
(7) Bates, T. S.; Charlson, R. J.; Gammon, R. H. *Nature* **1987**, *329*, 319.
(8) Legrand, M. R.; Delmas, R. J.; Charlson, R. J. *Nature* **1988**, *334*, 418.
(9) Rampino, M.; Volk, T. *Nature* **1988**, *332*, 63.
(10) Kerr, R. A. *Science* **1988**, *240*, 393.
(11) Lindley, D. *Nature* **1988**, *332*, 483.
(12) Martin, D.; Jourdain, J. L.; Laverdet, G.; LeBras, G. *Int. J. Chem. Kinet.* **1987**, *19*, 503.
(13) Barnes, I.; Becker, K. H.; Carlier, P.; Mouvier, G. *Int. J. Chem. Kinet.* **1987**, *19*, 489.
(14) Chatfield, R. B.; Crutzen, P. J. *J. Geophys. Res.*, in press.
(15) Wallington, T. J.; Atkinson, R.; Winer, A. M.; Pitts, J. N., Jr. *J. Phys. Chem.* **1986**, *90*, 4640.
(16) Wallington, T. J.; Atkinson, R.; Winer, A. M.; Pitts, J. N., Jr. *J. Phys. Chem.* **1986**, *90*, 5393.

0022-3654/90/2094-5839$02.50/0

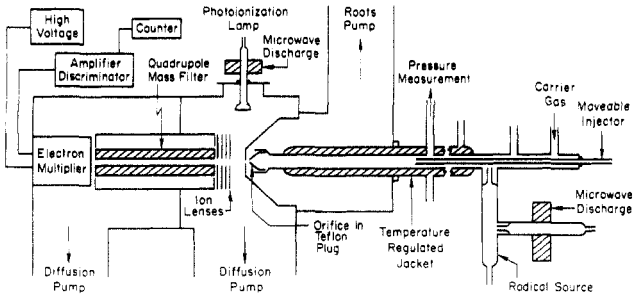

Figure 1. Apparatus schematic showing the discharge flow tube and photoionization mass spectrometer detector.

and IO are low enough not to compete with the OH oxidation. Moreover, the OH oxidation of other sulfur compounds (CH_3SH, CH_3SSCH_3), whose emissions into the atmosphere are smaller than that of DMS, is also thought to lead to CH_3S.[21-24] Also, it is possible that the reaction of CH_3SSCH_3 (DMDS) with NO_3 leads to CH_3S.[19]

It is then very likely that CH_3S is an important intermediate in the atmospheric oxidation of some reduced sulfur compounds, and it is necessary to understand the reactions of CH_3S with its most likely atmospheric oxidants, which include O_2, NO_2, and O_3.

The present work reports laboratory measurements of the reaction

$$CH_3S + NO_2 \rightarrow \text{products} \qquad (1)$$

This reaction has already been studied by Balla et al.[25] and Tyndall and Ravishankara[26] using flash photolysis systems with laser-induced fluorescence (LIF) detection of CH_3S. They obtained rate constant values of (in cm^3 $molecule^{-1}$ s^{-1}) $k_1 = (10.9 \pm 1) \times 10^{-11}$ and $(6.1 \pm 0.9) \times 10^{-11}$, respectively. In light of the error limits given by these authors, the agreement between these two values is relatively poor, and a further measurement may prove useful to resolve this discrepancy. Balla et al. and Tyndall and Ravishankara have suggested that CH_3SO was a product of the reaction of CH_3S with NO_2 but did not rule out the formation of an adduct CH_3SNO_2. Tyndall and Ravishankara measured the yield of NO from reaction 1 to be 0.8 ± 0.2 and also observed that the NO rise had two components and interpreted the second component as being due to

$$CH_3SO + NO_2 \rightarrow CH_3SO_2 + NO \qquad (2)$$

By modeling the rise of NO, Tyndall and Ravishankara determined the rate constant of reaction 2 and obtained $k_2 = (8 \pm 5) \times 10^{-12}$ cm^3 $molecule^{-1}$ s^{-1}. Mellouki et al.[27] have studied the reaction of Cl with CH_3SH in the presence of NO_2 using a discharge flow tube with a mass spectrometer detector. Using a curve-fitting method, they obtained $k_2 = (3 \pm 2) \times 10^{-11}$ cm^3 $molecule^{-1}$ s^{-1}. Both of these determinations of k_2 are indirect and there is a significant amount of disagreement between them. CH_3SO was detected in our system and we have also measured k_2 by monitoring the decay of CH_3SO in the presence of NO_2.

CH_3SS and CH_3SSO were formed by secondary chemistry and were detected in our system. These radicals could be intermediates in the atmospheric oxidation of DMDS, and we have measured the rate constants for

$$CH_3SS + NO_2 \rightarrow CH_3SSO + NO \qquad (3a)$$

$$\rightarrow CH_3S(O)S + NO \qquad (3b)$$

$$CH_3SSO + NO_2 \rightarrow \text{products} \qquad (4)$$

Experimental Section

Apparatus. The experimental system, shown in Figure 1, is a modification to the flow tube photoionization mass spectrometer (PIMS) described by Murrells and Howard.[28] The goal of the changes was to improve the mass resolution of the system, which required using a bigger quadrupole filter.

The flow tube used was very similar to that of Murrells and Howard. We used a 2.54-cm-i.d. Pyrex tube. The tube had a 50-cm-long reaction region coated with halocarbon wax and surrounded by a temperature-regulated jacket. A threaded Teflon plug was inserted at the end of the flow tube. A hole was drilled in the 0.5-mm-thick wall at the end of the plug. Different hole diameters (typically 5 mm) were used to obtain average flow velocities, v, between 1800 and 2500 cm s^{-1}. Usually, atoms were produced by a microwave discharge and reacted with a stable molecule to make the radical of interest in a sidearm reactor, which was also coated with halocarbon wax. The radical decay was monitored under pseudo-first-order conditions. NO_2 flowed through the moveable injector, whose position determined the reaction time. Helium was used as the carrier gas. The reactor pressures used were between 1 and 3 Torr and were measured through a port at the center of the reaction region by a 10-Torr full-scale capacitance manometer. The flow rate of the carrier gas was measured by linear mass flowmeters calibrated with a wet test meter. The flow rates of the other chemicals used here, such as the stable sulfur molecules and the NO_2, were measured by the pressure rate of change method. In the case of NO_2, a correction was made to account for the dimerization equilibrium and was typically less than 2% of the calculated flow.

The flow tube effluents were sampled into the ionization chamber through a beveled sampling pinhole 0.5 mm in diameter drilled in a 0.5-mm-thick molybdenum disk. This is a change from Murrells and Howard's system,[28] where the flow tube effluents were ionized before being sampled into the first chamber of the mass spectrometer. The vacuum UV ionizing radiation used most of the time was hydrogen Lyman α (10.2 eV),[29] produced by flowing pure H_2 through a microwave discharge operated at 50 W. Some H_2 emission was also produced in this lamp. Mixtures of H_2 in He were also tried but were found to be less intense sources of Lyman α radiation than pure H_2. The optimum pressure of H_2 in the lamp was found to be approximately 0.6 Torr. Krypton (10.03 and 10.64 eV) and oxygen (9.5 eV) emission lamps were also obtained by flowing either pure Kr at a pressure of 0.8 Torr or a mixture of 7% O_2 in He at a pressure of 0.8 Torr through a microwave discharge. The use of krypton or oxygen in the discharge gave ion signals 7 and 15 times less intense, respectively, than with pure H_2. A MgF_2 crystal window was used on the vacuum UV lamp. The presence of sulfur compounds resulted in a brown film being deposited on the outside of the windows. This caused the ion signals to decrease with time. Typically, the signal decreased by a factor of 2 after about 100 h of exposure. This decrease was not fast enough to interfere with our measurements. The windows were cleaned regularly in methanol or replaced to restore the sensitivity.

The ions formed were focused into the quadrupole mass filter by a set of four ion lenses whose voltages were adjusted to optimize the signals. The quadrupole filter was 22 cm long and was located

(17) Tyndall, G. S.; Burrows, J. P.; Schneider, W.; Moortgat, G. K. *Chem. Phys. Lett.* **1986**, *130*, 463.
(18) Atkinson, R.; Aschmann, S. M.; Pitts, J. N., Jr. *J. Geophys. Res.* **1988**, *93*, 7125.
(19) Dlugokencky, E. J.; Howard, C. J. *J. Phys. Chem.* **1988**, *92*, 1188.
(20) Niki, H.; Maker, P. D.; Savage, C. M.; Breitenbach, L. P. *Int. J. Chem. Kinet.* **1983**, *15*, 647.
(21) Hatakeyama, S.; Akimato, H. *J. Phys. Chem.* **1983**, *87*, 2387.
(22) Grosjean, D. *Environ. Sci. Technol.* **1984**, *18*, 460.
(23) Wine, P. H.; Kruetter, N. M.; Gump, C. A.; Ravishankara, A. R. *J. Phys. Chem.* **1981**, *85*, 2660.
(24) MacLeod, H.; Jourdain, J. L.; Poulet, G.; LeBras, G. *Atmos. Environ.* **1984**, *18*, 2621.
(25) Balla, R. J.; Nelson, H. H.; McDonald, J. R. *Chem. Phys.* **1986**, *109*, 101.
(26) Tyndall, G. S.; Ravishankara, A. R. *J. Phys. Chem.* **1989**, *93*, 2426.
(27) Mellouki, A.; Jourdain, J. L.; LeBras, G. *Chem. Phys. Lett.* **1988**, *148*, 231.
(28) Murrells, T. P.; Howard, C. J. *Int. J. Chem. Kinet.*, submitted.
(29) Samson, J. A. R. *Techniques of Vacuum Ultraviolet Spectroscopy*; Wiley: New York, 1967; pp 131, 144, 161.

TABLE I: Ionization Potentials (IP) of Molecules and Radicals Relevant to This Study

compd	IP,[a] eV	compd	IP,[a] eV
S	10.5	C_2H_5SH	9.29
SO	10.3	CH_3SCH_3	8.70
SO_2	12.4	$(CH_3)_2SO$	9.01
S_2	9.36	$CH_3SC_2H_5$	8.46
HS	10.5	$CH_3S(O)C_2H_5$	8.89
H_2S	10.46	$(CH_3S)_2$	8.97
CH_2S	9.34	CH_3	9.83
CH_3S	7.53	C_2H_5	8.39
CH_3SO	7.6–8.5[b]	NO	9.26
CH_3SH	9.44	NO_2	<9.62
C_2H_5S	7.04	HONO	11.3

[a] From ref 30, with thermochemical values from Benson,[31] except $\Delta H_f°_{298}(CH_3S)$, taken from Shum and Benson.[32] [b] A major discrepancy exists in the literature on $\Delta H_f°_{298}(CH_3SO)$.[33]

in the second chamber of the mass spectrometer, whereas the previous mass filter was 10.5 cm long and was located in the first chamber. The holes at the center of the lenses were beveled to minimize the amount of UV light scattered into the multiplier. The quadrupole resolution $m/\Delta m$, where Δm is the width at half-maximum, was 200 at mass 48. The CH_3S and CH_3SH peaks were very well resolved, and when no CH_3S was formed in the flow tube, the mass 47/mass 48 signal ratio was $<10^{-4}$. An electron multiplier was used as a detector. The pressure in the chamber housing the quadrupole filter and the detector was approximately 3×10^{-6} Torr.

Our system was extremely sensitive to those stable sulfur molecules whose ionization potentials were less than the energy of the vacuum UV radiation used. Table I reports the ionization potentials of the relevant molecules and radicals for which they are known or can be calculated by using thermochemical data. The detection limit of all the stable reduced sulfur molecules we used was about 10^6 molecules cm^{-3} in the flow tube. Specifically, detection limits were 0.7, 2, and 3×10^6 molecule cm^{-3} for CH_3SSCH_3, $CH_3SC_2H_5$ (ethyl methyl sulfide, EMS) and CH_3SH (methanethiol), respectively. In general we found that, within a factor of 2, the signal intensity of a sulfur compound in a given concentration was proportional to the number of sulfur atoms it contained. The detection limit of the reduced sulfur radicals used here have not been measured, but we expect them to be as low and possibly lower than those of the stable molecules mentioned above. The PIMS could detect most sulfur radicals present in the reactor. In general, the only reduced sulfur radicals that we could not detect at their parent ion masses were those whose ionization potentials were too high and weakly bound radicals such as CH_3SO_2, which may be photolyzed by the UV radiation.

Radical Sources. Reaction 5 was the main source of CH_3S used in this study. The Cl atoms were formed by flowing a

$$Cl + CH_3SH \rightarrow HCl + CH_3S \quad (5a)$$

$$\rightarrow HCl + CH_2SH \quad (5b)$$

mixture of 0.9% CCl_4 in He through a microwave discharge. A 3% Cl_2 in He mixture was also used to make Cl atoms for some measurements. Source conditions were adjusted so that >95% of the chlorine atoms were consumed in the side arm by reaction 5. Nesbitt and Leone[34] and Mellouki et al.[27] report $k_5 = 1.8 \times 10^{-10}$ and 1.1×10^{-10} cm^3 $molecule^{-1}$ s^{-1}, respectively. Nesbitt and Leone[35] report that channel 5b accounts for less than 2% of reaction 5, which is therefore a good kinetics source of CH_3S.

Reaction 6 was also used as a source of both CH_3S and CH_3SO:

$$O + CH_3SSCH_3 \rightarrow CH_3S + CH_3SO \quad (6a)$$

$$\xrightarrow{M} CH_3S(O)SCH_3 \quad (6b)$$

Oxygen atoms were produced for most of the measurements by flowing a mixture of 4% O_2 in He through a microwave discharge. Reaction 7 was also used as a source of O atoms, in which case

$$N + NO \rightarrow N_2 + O \quad (7)$$

N atoms were produced by flowing a mixture of 1% N_2 in He through a microwave discharge. The product of channel 6b was detected at mass 110, but the signal at mass 110 was less than 1% of the CH_3SO signal. The rate constant of reaction 6 is greater than 1×10^{-10} cm^3 $molecule^{-1}$ s^{-1}.[36]

The CH_3S was also produced by the photolysis of DMDS:

$$CH_3SSCH_3 + h\nu\ (253.7\ nm) \rightarrow CH_3S + CH_3S \quad (8)$$

This was done by inserting a mercury pen ray lamp in the sidearm reactor. The CH_3S signal was rather low when this source was used, and very few data were obtained with it. To produce CH_3S radicals, we also tested reaction 9:

$$Cl + CH_3SSCH_3 \rightarrow CH_3S + CH_3SCl \quad (9a)$$

$$\rightarrow HCl + CH_3SSCH_2 \quad (9b)$$

but assuming that the ionization efficiency for CH_3SSCH_2 at mass 93 is twice that of CH_3S at mass 47, channel 9b accounts for about 30% of reaction 9 and this source was not used for our rate constant measurements. By flowing DMDS through the injector and by looking at the rise of CH_3S, we could estimate that $k_9 > 1 \times 10^{-10}$ cm^3 $molecule^{-1}$ s^{-1}.

CH_3SO produced in reaction 6 was used to measure k_2. Reaction 10 was also used as a source of CH_3SO. C_2H_5SO, which

$$O + CH_3SC_2H_5 \rightarrow CH_3SO + C_2H_5 \quad (10a)$$

$$\rightarrow CH_3 + C_2H_5SO \quad (10b)$$

was produced by channel 10b, could not be detected at mass 77 because the natural occurrence of ^{13}C and ^{33}S in $CH_3SC_2H_5$ resulted in a strong background signal at mass 77, whose intensity was about 4% of the signal at mass 76. Slagle et al.[37] showed a linear correlation between the rate constants of the reactions of O with R_1SR_2 (where R_1 and R_2 are H or alkyl groups) and the ionization potential of R_1SR_2. From Table I and the correlation of Slagle et al., we estimate $k_{10} \approx 1.5 \times 10^{-10}$ cm^3 $molecule^{-1}$ s^{-1}.

CH_3SS was found to be generated in the radical source reactor whenever CH_3S was produced, which suggested that CH_3SS was probably formed by some secondary chemistry involving CH_3S. We tried to make CH_3SS by reaction 11, but this attempt was

$$\overbrace{CH_2SCH_2} + CH_3S \rightarrow CH_3SS + C_2H_4 \quad (11)$$

not successful, and we assign an upper limit of 3×10^{-14} cm^3 $molecule^{-1}$ s^{-1} to k_{11}. We used reaction 3 of CH_3SS with NO_2, to make CH_3SSO.

We attempted to detect CH_3SO_2 formed in reaction 2. Interference from CH_3SS at mass 79 made this effort inconclusive. We tried to react $CH_3S(O)CH_3$ with O atoms, as this reaction may give CH_3SO_2 and CH_3. We did see a signal rise at mass 15, characteristic of CH_3, but detected nothing at mass 79, from which we concluded that CH_3SO_2 was not detectable at mass 79 in our system.

We tested for the possibility of radical generation by reaction of the precursor gases with NO_2 by turning off the microwave

(30) Levin, R. D.; Lias, S. G. *Ionization Potential and Appearance Potential Measurements*; Natl. Stand. Data Ser., Natl. Bur. Stand. No. 71, Washington, DC, 1982.
(31) Benson, S. W. *Chem. Rev.* **1978**, *78*, 23.
(32) Shum, L. G. S.; Benson, S. W. *Int. J. Chem. Kinet.* **1983**, *15*, 433.
(33) If calculated from the data of Benson,[31] $\Delta H_f°_{298}(CH_3SO) = -16.4$ kcal mol^{-1}. This implies an S–O bond energy of 107 kcal mol^{-1} in CH_3SO. Swarts et al. (Swarts, S. G.; Becker, D.; DeBolt, S.; Sevilla, M. D. *J. Phys. Chem.* **1989**, *93*, 155) estimate this energy to be 86 kcal mol^{-1}, which yields $\Delta H_f°_{298}(CH_3SO) = 4.6$ kcal mol^{-1}. Using the appearance potential of $C_2H_5^+$ from $CH_3S(O)C_2H_5$,[30] one finds $\Delta H_f°_{298}(CH_3SO) = 7.4 \pm 4.6$ kcal mol^{-1}. Benson's value of the S–C bond strength in DMSO[31] used to obtain the first value is probably in error by about 20 kcal mol^{-1}, and the ionization potential of CH_3SO is probably closer to 7.6 eV.
(34) Nesbitt, D. J.; Leone, S. R. *J. Chem. Phys.* **1980**, *72*, 1722.
(35) Nesbitt, D. J.; Leone, S. R. *J. Chem. Phys.* **1981**, *75*, 4949.
(36) Baulch, D. L.; Cox, R. A.; Hampson, R. F.; Kerr, J. A.; Troe, J.; Watson, R. T. *J. Phys. Chem. Ref. Data* **1984**, *13*, 1259.
(37) Slagle, I. R.; Graham, R. E.; Gutman, D. *Int. J. Chem. Kinet.* **1976**, *8*, 451.

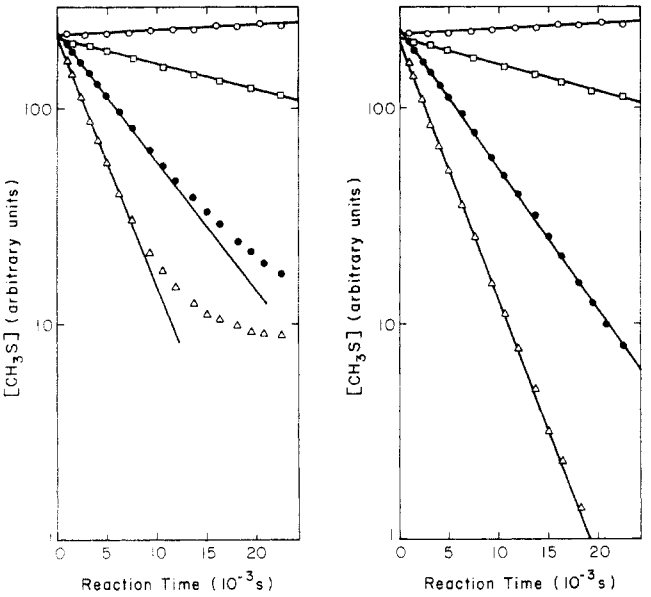

Figure 2. Left: $CH_3S + NO_2$ decay plots, with $[CH_3S]$ monitored at mass 47. CH_3S source: Cl/CH_3SH. $T = 297$ K, $P = 1$ Torr, $v = 2270$ cm s^{-1}. A signal of 100 corresponds to $[CH_3S] \approx 2 \times 10^{10}$ molecules cm^{-3}. $[NO_2]$ (10^{12} molecules cm^{-3}) = 0 (○), 1.34 (□), 2.67 (●), 5.56 (△). Right: same data as left panel, after subtraction of the contribution of the CH_3SSO fragment to the mass 47 signal (see text).

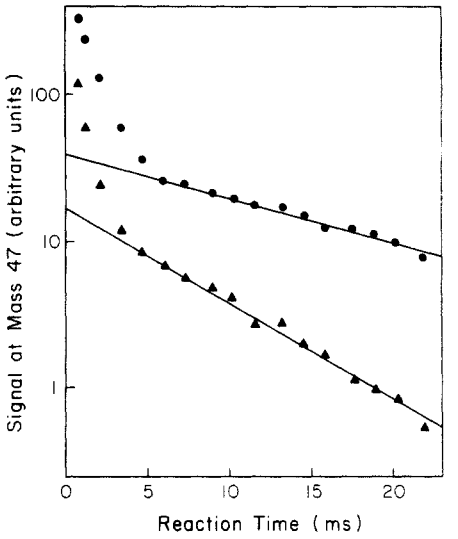

Figure 3. $CH_3S + NO_2$ decay plots at high $[NO_2]$, showing the linear region at long reaction time, which is used to measure the rate constant of the $CH_3SSO + NO_2$ reaction. Source: Cl/CH_3SH, $T = 296$ K, $P = 1$ Torr, $v = 2310$ cm s^{-1}. $[NO_2]$ (10^{13} molecules cm^{-3}) = 1.46 (●); 4.11 (▲).

discharge and searching for radicals with the mass spectrometer. No detectable background signals were observed, indicating no significant radical generation.

The helium (≥99.999%), hydrogen (≥99.999%), oxygen (≥99.97%), DMDS (≥99%), EMS (≥99%), and CCl_4 (≥99.9%) were used without further purification. The CH_3SH purity was stated as 99.5%, but we found that it contained about 1% DMDS and small amounts of DMS. The DMDS may have been formed by the dimerization of CH_3SH on the cylinder walls. The impurity levels of DMDS and DMS were reduced by about a factor of 10 by vacuum distillation. The NO_2 was prepared by reacting purified NO in excess O_2 at about 1000 Torr and purified by trap-to-trap distillation in excess O_2.

Results

CH_3S, CH_3SS, and $CH_3SSO + NO_2$. All the kinetic measurements were made under pseudo-first-order conditions in excess NO_2. We then have, for example for CH_3S:

$$\ln \{[CH_3S]/[CH_3S]_0\} = -k_1^I t = -k_1[NO_2]t$$

where k_1^I is the first-order rate constant and k_1 is the second-order rate constant for reaction 1. The reaction time t is the reaction distance divided by the average flow velocity. Since we found that the ion current at mass 48 was proportional to $[CH_3SH]$ in the flow tube, we assume that the CH_3S^+ signal at mass 47 is proportional to $[CH_3S]$ in the flow tube. Therefore, a plot of the decay of ln (CH_3S^+ signal at mass 47) vs reaction time should yield a straight line of slope $-k^I$. The second-order rate constant k is then the slope of a k^I vs $[NO_2]$ plot.

However, as shown in Figure 2, left, we found that the CH_3S decay plots were curved. The initial slopes of the plots gave a rate constant of about 5×10^{-11} cm^3 $molecule^{-1}$ s^{-1}, close to the value of Tyndall and Ravishankara.[26] However, we have tried to understand the cause of the curvature, which was observed under a wide variety of conditions and had the following characteristics. The curvature was observed when the source of CH_3S was (a) the reaction of Cl with CH_3SH, with Cl_2 or CCl_4 as a source of Cl, (b) the reaction of O with DMDS, with O_2 or the reaction of N with NO as a source of O, and (c) the photolysis of DMDS. The curvature was negligible at the lowest $[NO_2]$ used but increased with increasing $[NO_2]$. The curvature was the most pronounced when the flow velocity in the source reactor was slowest and could be minimized by making the CH_3S radicals in the flow tube, i.e., by flowing the sulfur precursor through a port in the flow tube upstream from the sidearm. The concentrations of CH_3S or of the sulfur precursor did not have much effect on the curvature. When the reaction of Cl with CH_3SH or the photolysis of DMDS was used as a source reaction, it was observed as shown on Figure 3 that after the initial curvature, the decay plots became linear at long reaction times for relatively high $[NO_2]$. The slope of this linear part was found to be proportional to $[NO_2]$, which is consistent with the presence of a species that was detected at mass 47 and that reacted with NO_2. When the reaction of O with DMDS was used as a source, it was observed that after the initial curved decay, the signal at mass 47 was actually rising to reach a maximum before decreasing again in a nonlinear manner. The maximum shifted to shorter reaction times as the $[NO_2]$ was increased.

We did not attribute the curvature to CH_3S regeneration in a $CH_3S + NO_2$ mixture, because Balla et al.[25] and Tyndall and Ravishankara[26] observed linear CH_3S decay plots using LIF detection of CH_3S and because there is no reasonable mechanism that can support such regeneration. Since we have used several source reactions for CH_3S, an artifact due to our detection method seems to be the most likely cause of the curvature, but we have investigated the following four possibilities: (1) unusual wall effects; (2) the detection at mass 47 of some species other than CH_3S; (3) some secondary chemistry regenerating CH_3S; (4) the photoionization of a parent molecule that fragments to yield a mass 47 ion.

With regard to (1), Wang et al.[38] observed that the wall loss of HS decreased with increasing temperature. One may expect CH_3S to behave similarly, and we performed measurements at 100 °C but did not observe any significant modifications in the curvature. With regard to (2), the species other than CH_3S that we could expect to detect at mass 47 in our system include CH_2SH, CCl, and HONO. CH_2SH could be formed only when the reaction of Cl with CH_3SH was used as a source of CH_3S, and we do not expect CH_3S to isomerize to the less stable CH_2SH form. CCl would appear only when CCl_4 was used as a Cl precursor. HONO is unlikely to be formed and detected because NO_2 is a poor hydrogen abstractor and HONO cannot be ionized by the vacuum UV wavelengths used (see Table I).

Possibilities (3) and (4) and the observation that source conditions strongly affect the curvature suggest the investigation of the source chemistry. The chemistry of the $Cl + CH_3SH$ reaction

(38) Wang, N. S.; Lovejoy, E. R.; Howard, C. J. *J. Phys. Chem.* **1987**, *91*, 5743.

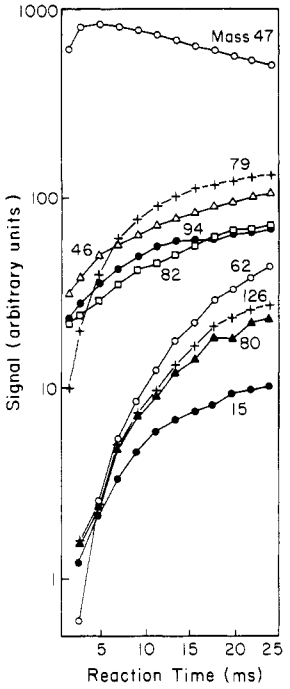

Figure 4. Chemistry of the Cl/CH_3SH source. T = 298 K, P = 1.1 Torr, v = 2320 cm s^{-1}. $[CH_3SH] = 4.3 \times 10^{12}$ molecules cm^{-3}. Mass assignments are as follows: 47, CH_3S; 79, CH_3SS; 46, CH_2S; 82, CH_3SCl; 94, $(CH_3S)_2$; 62, $(CH_3)_2S$; 126, CH_3SSSCH_3; 80, CH_3SSH; 15, CH_3. The maximum $[CH_3S] = (2 \pm 1) \times 10^{11}$ molecules cm^{-3}.

(the simplest source) was studied by flowing CH_3SH through the moveable injector and a CCl_4/He mixture through the microwave discharge. Signals were observed at numerous masses, and these are plotted as a function of reaction time on Figure 4. The following mass assignments are consistent with the chemistry we observed and, in the case of masses 82 and 94, with the intensities of the isotope peaks at masses 84, 95, and 96: 47, CH_3S; 79, CH_3SS; 46, CH_2S; 82, CH_3SCl; 94, CH_3SSCH_3. The following mass assignments are made on a tentative basis: 62, CH_3SCH_3; 126, CH_3SSSCH_3; 80, CH_3SSH; 15, CH_3.

To detect as many as possible of the species that are formed in the source, the CH_3S concentration was maximized for this source study. We estimated the maximum $[CH_3S]$ of Figure 4 by three different methods: (a) measuring $[CH_3SH]$ with the discharge on and off and assuming that the difference was due solely to CH_3S; (b) assuming that CH_3S and CH_3SH are detected with the same efficiencies; (c) assuming that one chlorine atom is produced from each CCl_4 molecule going through the microwave discharge. Despite their crudity, these three methods give results in the range (1.5–2.5) $\times 10^{11}$ molecules cm^{-3}, and while keeping in mind that the following value is only an approximation, we estimate that $[CH_3S]_{max} \approx (2 \pm 1) \times 10^{11}$ molecules cm^{-3}.

Figure 4 shows CH_3S being formed and then decaying. Using lower initial $[CH_3S]$ showed a sharp decline in the rate of decay, which is consistent with the decay being second order in CH_3S and being mainly due to the self-reaction of CH_3S. Reaction 12

$$CH_3S + CH_3S \xrightarrow{M} CH_3SSCH_3 \quad (12a)$$

$$\rightarrow CH_2S + CH_3SH \quad (12b)$$

has been investigated by Graham et al.,[39] who report the high-pressure limit of $k_{12} = 4.1 \times 10^{-11}$ cm^3 $molecule^{-1}$ s^{-1}. Tycholiz and Knight[40] have measured the high-pressure limit of the branching ratio of reaction 12 and report $k_{12b}/k_{12a} = 0.04$, from which we deduce $k_{12b} = 1.6 \times 10^{-12}$ cm^3 $molecule^{-1}$ s^{-1}. It is reasonable to assume that the formation of CH_2S in our system is due to reaction 12b. However, if we use our $[CH_3S]_{max}$ estimate, our observed decay of CH_3S gives $k_{12} \approx 8 \times 10^{-11}$ cm^3 $molecule^{-1}$ s^{-1}. Similarly, the reaction rate coefficient derived from the CH_2S and DMDS products appearance rates is $k_{12} \approx 5 \times 10^{-11}$ cm^3 $molecule^{-1}$ s^{-1}. Assuming that CH_2S and DMDS are detected with the same efficiencies, we get $k_{12b} \approx 3 \times 10^{-11}$ cm^3 $molecule^{-1}$ s^{-1}. These values are in sharp disagreement with what could be expected at 1 Torr from Graham et al. and Tycholiz and Knight.

More recently, Martin et al.[41] have used $k_{12b} = 6.0 \times 10^{-11}$ cm^3 $molecule^{-1}$ s^{-1}, but it is not clear what this number is based on. An error in our estimation of our radical concentration cannot explain the discrepancy between our value of k_{12} and that obtained by Graham et al., as we would need $[CH_3S]_0 > \approx 5 \times 10^{12}$ molecule cm^{-3}, which is impossible as this is higher than $[CH_3SH]_0$. We must then conclude either that Graham et al. are in error, which is possible because they used an indirect method to measure k_{12}, or that other reactions, such as wall reactions, consume CH_3S and produce CH_2S in our system.

The formation mechanism of CH_3SS is another problem. Reaction 12c cannot satisfactorily explain the formation of the

$$CH_3S + CH_3S \rightarrow CH_3SS + CH_3 \qquad \Delta H = -9.3 \text{ kcal mol}^{-1} \quad (12c)$$

CH_3SS, because the appearance of CH_3SS occurs on a time scale different from that of CH_2S and of CH_3SSCH_3. The reaction of CH_3S with elemental sulfur on the walls of the side arm reactor:

$$CH_3S + S_{wall} \rightarrow CH_3SS \qquad \Delta H = -13.7 \text{ kcal mol}^{-1} \quad (13)$$

is a possible explanation for the formation of CH_3SS. Radford[42] actually used a similar reaction and made HS by reacting H atoms with elemental sulfur deposited on a reactor wall. The suggestion that CH_3SS is formed by a wall reaction is also supported by the observation that cleaning the wall by exposing it to a stream of oxygen atoms for a day decreased the amount of CH_3SS formed by about a factor of 2. However, the exact source of CH_3SS is not important to our study, although we believe this radical is associated with the curvature of the CH_3S decay plots as described below.

With regard to possibility (3), since the curvature depends on $[NO_2]$, we examined the possibility of a reaction such as

$$A + NO_2 \rightarrow CH_3S + B \quad (14)$$

where A is a species that is present in our reactor and that contains the CH_3S group. Among the detectable species containing the CH_3S fragment, it was observed that the product at mass 79 (CH_3SS) reacted with NO_2. However, it is unlikely that CH_3S is a product of this reaction because the only channel that could be exothermic would also give SONO, which we did not detect at mass 78. More likely products are CH_3SSO and $CH_3S(O)S$, as confirmed by the appearance of a signal at mass 95.

With regard to (4), a compound could be photolyzed by the vacuum UV radiation to give a CH_3S^+ fragment:

$$C + h\nu \ (\lambda = 121.6 \text{ nm}) \rightarrow CH_3S^+ + e^- + D \quad (15)$$

Among the compounds that we detected in our system, CH_3SSO is the only one that could meet the following conditions: (a) it reacts with NO_2; (b) its reaction, (15), is exothermic; (c) its concentration depends on the source conditions. Indeed, its precursor, CH_3SS, is formed in the source in amounts that depend on the source conditions. Also, since HSO[43] and CH_3SO[26] are known to react with NO_2, CH_3SSO may also be expected to react with NO_2.

We now need to test that the reaction

$$CH_3SSO + h\nu \ (\lambda = 121.6 \text{ or } 130.5 \text{ nm}) \rightarrow CH_3S^+ + e^- + SO \quad (16)$$

(39) Graham, D. M.; Mieville, R. L.; Pallen, R. H.; Sivertz, C. *Can. J. Chem.* **1964**, *42*, 2250.
(40) Tycholiz, D. R.; Knight, A. R. *J. Am. Chem. Soc.* **1973**, *95*, 1726.
(41) Martin, D.; Jourdain, J. L.; LeBras, G. *Int. J. Chem. Kinet.* **1988**, *20*, 897.
(42) Radford, H. E. *J. Chem. Phys.* **1964**, *40*, 2732.
(43) Lovejoy, E. R.; Wang, N. S.; Howard, C. J. *J. Phys. Chem.* **1987**, *91*, 5749.

is responsible for the observed CH_3S decay plot curvature. We need to (a) establish that this is energetically possible, (b) derive an equation that predicts the concentration of CH_3SSO and its contributions to the mass 47 signal, and (c) perform the measurements required to check the validity of this model and, if it is valid, use it to correct the curvature of the mass 47 decay plots.

There is considerable uncertainty in the thermochemistry of the RSSO and RSO compounds.[33] Assuming a value of 85 kcal mol^{-1} for the S=O bond dissociation energy in CH_3SSO, we estimate $\Delta H_r°_{298} = -21$ kcal mol^{-1} for reaction 16 with the 121.6-nm (10.2 eV) radiation and $\Delta H_r°_{298} = -5$ kcal mol^{-1} with the 130.5-nm (9.5 eV) radiation. This shows that the reaction can take place under our conditions. The thermochemistry is even more favorable for this process if SO^- is formed, but we have no evidence to support this possibility. According to our model CH_3SSO is formed by reaction 3a and consumed by reaction 4. Then, assuming that wall loss rates are negligible compared to the rates of reaction with NO_2 and can be neglected, the integrated rate equation

$$[CH_3SSO] = [CH_3SS]_0 \frac{k_{3a}}{k_3 - k_4}(e^{-k_4[NO_2]t} - e^{-k_3[NO_2]t}) \qquad (17)$$

describes the time dependence of $[CH_3SSO]$.

CH_3SSO cannot be easily measured at mass 95 because of the interference from ^{95}(DMDS) formed by the recombination of CH_3S in reaction 12a and from $CH_3S(O)S$ formed in reaction 3b. However, we can measure $[CH_3SS]_0$ and k_3 by monitoring CH_3SS at mass 79. According to our model, we can also determine k_4 from the slopes of the linear parts of the mass 47 decay plots at long reaction times. To evaluate the contribution of CH_3SSO to the mass 47 signal, we also need to know Φ, the yield of CH_3S^+ from the absorption of a Lyman α photon by CH_3SSO, as well as k_{3a}. These last two parameters cannot be easily measured. However, our goal is to subtract $\Phi[CH_3SSO]$ from the mass 47 signal and the quantity $[\Phi k_{3a}/(k_3 - k_4)]$ can be regrouped as x. The parameter x can then be adjusted for each decay plot so that the subtraction of the CH_3SSO contribution to the mass 47 signal yields a linear plot. If our model is consistent with the chemistry taking place in our systems, x should not vary from one decay plot to another.

To obtain $[CH_3SS]_0$ (arbitrary units) and k_3, the decay of CH_3SS was monitored at mass 79 in excess NO_2 simultaneously with the decay of CH_3S. The plots of ln (signal at mass 79) vs reaction time were linear when the Cl + CH_3SH reaction was used as a source. When the reaction of O with DMDS, (6), was used as an source, the plots, after the initial decay, were observed to rise before decaying again, in a manner very similar to the CH_3S plots obtained with this source. This complex curvature was not well understood, and the initial slope was taken as a measurement of k^I in this case. The data on reaction 3 are summarized in the k^I vs $[NO_2]$ plot shown in Figure 5. The slope is $(1.8 \pm 0.02) \times 10^{-11}$ cm^3 $molecule^{-1}$ s^{-1}, where the error is 1σ based on precision only. Using uncertainties for the gas flow rates (±3%), temperature (±1%), pressure (±1%), flow-tube radius (±1%), and slope of the decay plots (±2%) and taking into account an evaluation of systematic errors, we obtain, at the 95% confidence level, $k_3 = (1.8 \pm 0.3) \times 10^{-11}$ cm^3 $molecule^{-1}$ s^{-1}.

The rate constant k_4 was measured by monitoring the signal at mass 47 at high $[NO_2]$, to make the linear part observable at long reaction times. The k^I vs $[NO_2]$ plot of reaction 4 data is shown in Figure 6 and yields a rate constant $k_4 = (4.5 \pm 0.3) \times 10^{-12}$ cm^3 $molecule^{-1}$ s^{-1}, where the error is 1σ based on precision only. Estimating the errors in a manner similar to k_3 with an error on the slope of the decay plots of ±6%, we get $k_4 = (4.5 \pm 1.2) \times 10^{-12}$ cm^3 $molecule^{-1}$ s^{-1} at the 95% confidence level. Using the measured values of k_3 and k_4 the factor x was then adjusted for each of the 25 decay plots obtained by using the Lyman α light source. The values of x were found to fall within the range 0.196 ± 0.008 (arbitrary units). This range is very narrow, and x can be considered constant. This supports the hypothesis that the photolysis of CH_3SSO gives a CH_3S^+ fragment. The mass 47 decay plots were corrected with eq 17 and the value of x just

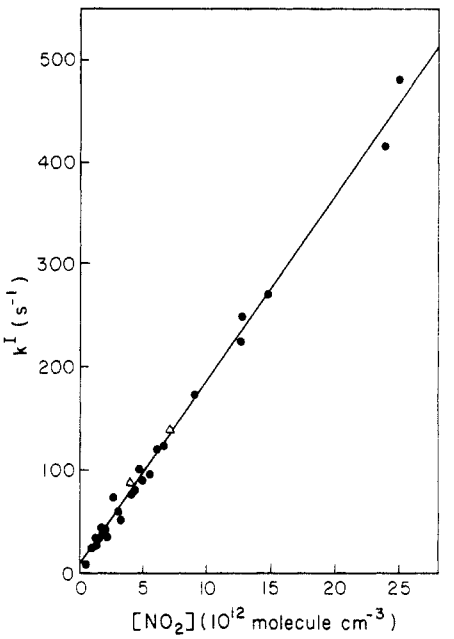

Figure 5. k^I vs $[NO_2]$ for the $CH_3SS + NO_2$ reaction. $T = (297 \pm 1)$ K, $P = 1$ Torr, slope = 1.8×10^{-11} cm^3 $molecule^{-1}$ s^{-1}. The CH_3SS is produced by secondary chemistry in the CH_3S source: Cl/CH_3SH (●); O/DMDS (△).

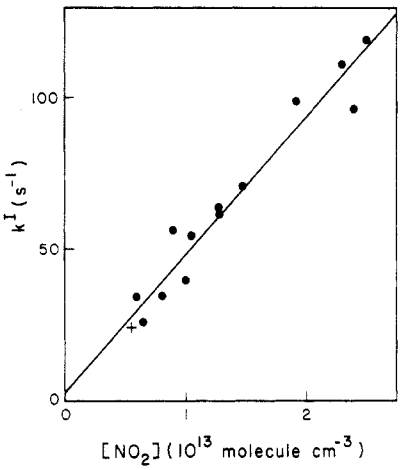

Figure 6. k^I vs $[NO_2]$ for the $CH_3SSO + NO_2$ reaction. $T = (297 \pm 1)$ K, $P = 1$ Torr, slope = 4.5×10^{-12} cm^3 $molecule^{-1}$ s^{-1}. The CH_3SSO is produced by secondary chemistry of the CH_3S source: Cl/CH_3SH (●); DMDS photolysis at 2357 Å (+).

determined. Three corrected plots are shown in Figure 2, right, and show linear decays of $[CH_3S]$ over a factor of up to 100 in concentration. To further test our explanation of the curvature, experiments were carried out using an O_2 discharge as a source of ionizing radiation. The absorption cross section of CH_3SSO and Φ probably decrease between 10.2 (H_2 discharge) and 9.5 eV (O_2 discharge), and we should expect x to change. With an O_2 discharge, the photolysis of CH_3SSO was slightly less efficient, as we measured $x = 0.143 \pm 0.007$. This is also consistent with the suggestion that reaction 16 is the cause of the curvature observed when the Cl + CH_3SH or the DMDS photolysis sources are used. The fact that this reaction can be driven by 9.5-eV radiation implies that the S=O bond energy in CH_3SSO is ≤90 kcal mol^{-1} (assuming a one-photon process).

The proposed explanation of the curvature of the CH_3S decay plots observed when the Cl + CH_3SH source was used does not account for the stronger and more complex curvature observed when the O + DMDS source, whose chemistry is detailed later on, was used to produce CH_3S. This could be because this source reaction produces two radicals, which may lead to more complex secondary chemistry and possibly another compound that gives

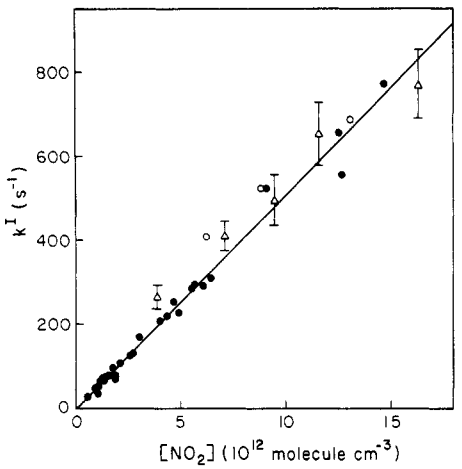

Figure 7. k^1 vs $[NO_2]$ for the $CH_3S + NO_2$ reaction. $T = (297 \pm 1)$ K, $P = 1$ Torr (△, O/DMDS source; ●, Cl/CH_3SH source) or 3 Torr (○, Cl/CH_3SH source), slope = 5.1×10^{-11} cm^3 $molecule^{-1}$ s^{-1} (fit not including 3-Torr data). The k^1 values obtained with the O/DMDS source are the initial slopes of the curved decay plots, which results in the large uncertainties shown.

a CH_3S^+ fragment. It is also possible that this reaction directly produces CH_3SSO and CH_3. This CH_3SSO would cause a curvature, although it would have different characteristics. However, we could detect neither of these radicals because CH_3SSO could not be observed at mass 95, due to the interference of ^{95}(DMDS) and because our detection limit for CH_3 is very high. The initial slopes of the decay plots are taken as a measurement of k_1^1, and due to the large curvature, these measurements are somewhat less accurate than, although totally consistent with, those performed with the $Cl + CH_3SH$ source.

A plot of the k_1^1 vs NO_2 data is shown in Figure 7. A least-squares fit of the 1-Torr data gives $k_1 = (5.1 \pm 0.1) \times 10^{-11}$ cm^3 $molecule^{-1}$ s^{-1}, where the error is 1σ on the basis of precision only. Including an evaluation of various errors similar to that of k_3, we get $k_1 = (5.1 \pm 0.9) \times 10^{-11}$ cm^3 $molecule^{-1}$ s^{-1} at 1 Torr at the 95% confidence level. Three points measured at 3 Torr of pressure are also shown in Figure 7, and these are consistent with the results obtained at 1 Torr.

$CH_3SO + NO_2$. When the $Cl + CH_3SH$ reaction or the photolysis of DMDS was used as a source, the decay of CH_3S in excess NO_2 was accompanied by the appearance of a signal at mass 63, which we assigned to the CH_3SO^+ ion. NO could also be monitored at mass 30. The rise of NO had at least two components, as observed by Tyndall and Ravishankara,[26] suggesting that CH_3SO also reacts with NO_2 to give NO and presumably CH_3SO_2, which we could not detect.

The decay of CH_3SO formed in the reactions of O with DMDS, (6a), or with EMS, (10a), was monitored in excess NO_2. In the case of reaction 6a, an initial rise in CH_3SO was observed, due to the reaction of NO_2 with CH_3S, which was also produced in reaction 6a, followed by a slightly curved decay. The decay parts of the plots were slightly curved at long reaction times. They became flatter and seemed to level off at high $[NO_2]$. The arbitrary subtraction of a constant background from the signal made the decay part of the plots linear. For a given set of source conditions, this background varied within a factor of about 1.5 for a set of decay plots, but it was very sensitive to the source conditions.

The chemistry of the O + DMDS source was investigated in the same manner as the $Cl + CH_3SH$ source, i.e., by adding DMDS through the injector to a stream of O atoms at a relatively high radical concentration. The ratio of the CH_3S and CH_3SO signals was initially 1.73, but the observed second-order decay of CH_3S was about 3 times faster than the second-order decay of CH_3SO, resulting in maximum signals (in arbitrary units) of 160 for CH_3SO and 232 for CH_3S. Signals were observed to rise at the following masses (maximum intensities given in parentheses): 64 (100), 126 (decay, then rise to 62), 79 (48), 46 (42), 62 (20), 48 (9), and 15 (3). Since SO_2 cannot be detected with 10.2-eV radiation, mass 64 could be S_2 but is probably CH_3SOH. The contribution of $^{64}(CH_3SO)$ to this signal was negligible. Masses 79, 46, 62, 48, and 15 were assigned to CH_3SS, CH_2S, CH_3SCH_3, CH_3SH, and CH_3 as before, and mass 126 could be CH_3SSSCH_3 and also $CH_3S(O)S(O)CH_3$. Mass 62 could be CH_3SCH_3 but probably has a contribution from CH_2SO. A very small signal whose variations with time were within the noise level was also observed at mass 110 and is assigned to $CH_3S(O)SCH_3$. These observations are consistent with a source chemistry that includes reactions 6, 12, 13, and

$$CH_3SO + CH_3SO \rightarrow CH_3SOH + CH_2SO \quad (18a)$$

$$\rightarrow CH_3S(O)S(O)CH_3 \quad (18b)$$

and the cross reactions of CH_3S and CH_3SO. The reaction

$$CH_3SO + S_{wall} \rightarrow CH_3S(O)S \quad (19)$$

cannot be ruled out, although this could not be confirmed at mass 95 due to the strong interference of ^{95}(DMDS).

It is suggested that the curvature of the CH_3SO decay plots is due to the photolysis in the ionization region of one or more compounds that contain the CH_3SO fragment. Such possible compounds include CH_3SOH, $CH_3S(O)S(O)CH_3$, $CH_3S(O)SCH_3$, and $CH_3S(O)S$ formed in reactions 18, 6b, and 3b and also $CH_3S(O)S(O)$, which can be formed by the reaction of $CH_3S(O)S$ and CH_3SSO with NO_2, although no signal was detected at mass 111. Due to the uncertainty in the thermochemistry of CH_3SO and of these sulfur compounds in general, it is not possible to shorten the above list with thermochemical considerations. A detailed analysis of our data suggests that the curvature of the CH_3SO decay plots could be due to either or both of the following possibilities: (1) a stable molecule, such as CH_3SOH, $CH_3S(O)SCH_3$, or $CH_3S(O)S(O)CH_3$, is formed in the source, or (2) two or more species such as $CH_3S(O)S(O)$ and $CH_3S(O)S$ are formed in the reaction region and photolyzed in the ionization region to yield a CH_3SO^+ fragment. If these radicals are formed and consumed by different NO_2 reaction rates, the plot will have a smooth curvature as observed. A similar hypothesis serves also to explain the complex curvature of the CH_3S and CH_3SS decay plots mentioned earlier. However, since neither of the radicals in question could be detected (no signal at mass 111, and strong interference from DMDS isotopes at mass 95), this hypothesis could not be tested.

Since the O + DMDS source reaction also produces CH_3S, the initial mass 63 signal increase due to the formation of CH_3SO by the $CH_3S + NO_2$ reaction was taken into account. First the decay part of a plot was made linear by the subtraction of a constant background. Then the signal rise and decay were fitted to a biexponential of the form

$$[CH_3SO] = Ae^{-k_1[NO_2]t} - Be^{-k_2[NO_2]t} \quad (20)$$

Since the curvature was slight, the k_2^1 values obtained from the fits and those obtained directly from the initial slopes of the decay part of the mass 63 plots were different by less than 5%. The k_2^1 values obtained from the fit are reported in Figure 8.

The reaction of O with EMS was also used as a source of CH_3SO. The advantage of this source is that it should not produce CH_3S. Since CH_3SO is less reactive than CH_3S, the secondary chemistry was expected to be less important when this source was used. However, these CH_3SO decay plots, as shown in Figure 9, were slightly curved. The curvature was less pronounced than when the O + DMDS source was used. This source chemistry was investigated. The peak at mass 63 (maximum intensity in arbitrary units, 210) was observed to rise and decay, and rising signals were detected at the following masses: 29 (109), 64 (47), 15 (18), 48 (10), 46 (9), 47 (6), and 62 (3) (where the values in parentheses indicate maximum intensities in the same arbitrary units). These signals are assigned to C_2H_5, CH_3SOH, CH_3, CH_3SH, CH_2S, CH_3S, and CH_2SO, respectively. The presence of C_2H_5SO (mass 77) and CH_3SS (mass 79) could not be confirmed due to the strong interference from the EMS isotope peaks.

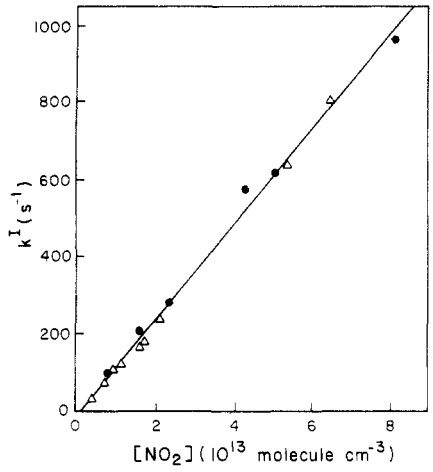

Figure 8. k^I vs $[NO_2]$ for the $CH_3SO + NO_2$ reaction. $T = (297 \pm 1)$ K, $P = 1$ Torr, slope = 1.2×10^{-11} cm^3 $molecule^{-1}$ s^{-1}. CH_3SO source: O/DMDS (△); O/EMS (●).

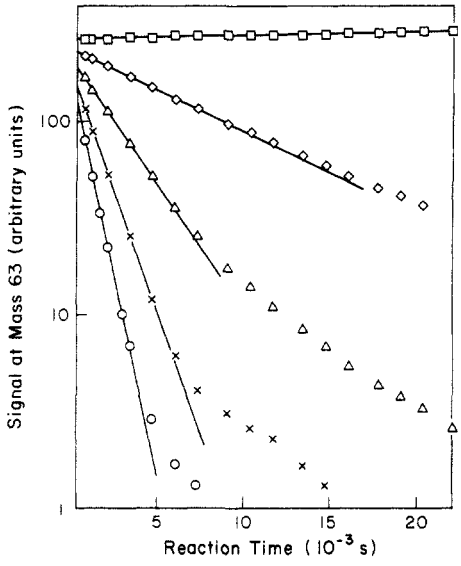

Figure 9. $CH_3SO + NO_2$ decay plots, with CH_3SO monitored at mass 63. CH_3SO source: O/EMS. $T = 297$ K, $P = 1$ Torr, $v = 2300$ cm s^{-1}. $[NO_2]$ (10^{13} molecules cm^{-3}) = 0 (□); 0.80 (◇); 2.33 (△); 4.33 (×); 8.16 (○).

However, assuming that CH_3SS and ^{79}(EMS) have similar instrument responses, CH_3SS can at the most be formed in amounts that are 4% of the amount of ^{79}(EMS). Since the study of the O + DMDS source showed that the ratio of our instrument responses to CH_3S and CH_3SO was 1.73, we conclude that the $[CH_3S]/[CH_3SO]$ ratio coming out of the source is <2%, and CH_3S should not interfere with our measurements. Since we do not know the relative instrument response to C_2H_5 and CH_3, we did not derive a branching ratio for reaction 10 from the signals at mass 29 and 15.

The source of the CH_3SO decay plot curvature when the O + EMS source was used was not understood. As with the O + DMDS source, the subtraction of a constant background did make the plots linear, but the magnitude of the background decreased strongly with increasing $[NO_2]$. However, the initial slopes of the plots and the slope of the plots made linear in the manner just described were different by less than 2% at low $[NO_2]$ and were identical at high $[NO_2]$. Furthermore, at high $[NO_2]$, the decay of $[CH_3SO]$ remained linear as $[CH_3SO]$ decreased by a factor of 10. The k_2^I values obtained with this source have been plotted vs $[NO_2]$ in Figure 8. The slope is $(1.2 \pm 0.02) \times 10^{-11}$ cm^3 $molecule^{-1}$ s^{-1}, and including an estimate of the total error, which includes a factor for the curvature of the decay plots, we get $k_2 = (1.2 \pm 0.25) \times 10^{-11}$ cm^3 $molecule^{-1}$ s^{-1} at the 95% confidence level.

The knowledge of k_1 and k_2 and of the relative instrument responses to CH_3S and CH_3SO, which was deduced from our study of the O + DMDS reaction, made it possible to measure the CH_3SO yield from the $CH_3S + NO_2$ reaction. This was done by using the $Cl + CH_3SH$ source reaction and monitoring the rise and decay of CH_3SO. Using an equation similar to (17) for $[CH_3SO]$ and including the wall losses of radicals, we get a CH_3SO yield of 1.07 ± 0.15. This means that the yield is unity, within experimental error.

Discussion

The reaction of CH_3S with NO_2 (1), has been previously investigated by Balla et al.,[25] who obtained $k_1 = (10.9 \pm 1) \times 10^{-11}$ cm^3 $molecule^{-1}$ s^{-1} from measurements performed between 1 and 200 Torr, and by Tyndall and Ravishankara,[26] who obtained $k_1 = (6.1 \pm 0.9) \times 10^{-11}$ cm^3 $molecule^{-1}$ s^{-1} from measurements between 17 and 140 Torr. Our value, $k_1 = (5.1 \pm 0.9) \times 10^{-11}$ cm^3 $molecule^{-1}$ s^{-1} at 1 Torr, is in reasonable agreement with the value of Tyndall and Ravishankara, who suggested that the high value obtained by Balla et al. could be due to the high $[CH_3S]$ used by those authors and also to the formation of a product that interferes with the detection of CH_3S. Tyndall and Ravishankara actually observed such an interference and attributed it to CH_3SO_2, formed in the reaction of CH_3SO with NO_2.

Our data were obtained with two different CH_3S sources that gave similar results. A very wide range of $[NO_2]$ of over a factor of 30 was used. Since we could detect a large number of sulfur compounds with a very low detection limit, we could examine the secondary chemistry and minimize the systematic errors that could result from it. We also made a detailed analysis of the cause of the curvature of the decay plots to make sure that it did not contribute a significant systematic error. This analysis showed that the curvature was not a significant problem, because taking the initial slope of the curved plots yielded a value within 2% of that obtained from the corrected plots.

Although the photoionization mass spectrometer detection system used here presented some problems caused by ion fragmentation, this technique does have some significant advantages. These advantages include an excellent sensitivity to many sulfur compounds, a selectivity to species having low ionization potentials, and a great versatility, as a large number of species can be detected. This last feature allowed the elucidation of some complex secondary and source chemistry.

The reaction of CH_3SO with NO_2, (2), has not been the subject of previous direct measurements. Using chemical modeling, Mellouki et al.[27] and Tyndall and Ravishankara[26] obtained $k_2 = (3 \pm 2) \times 10^{-11}$ and $k_2 = (8 \pm 5) \times 10^{-12}$ cm^3 $molecule^{-1}$ s^{-1}, respectively. Considering the large error limits given in these studies, both values agree with our result $k_2 = (1.2 \pm 0.25) \times 10^{-11}$ cm^3 $molecule^{-1}$ s^{-1}. Mellouki et al. used a discharge flow reactor with electron impact mass spectrometric detection and modeled the kinetics of the $Cl/Cl_2/CH_3SH/NO_2$ system. Their determination of k_2 was made by fitting the NO^+ (mass 30) and SO_2^+ (mass 64) signals. However, their reaction mechanism is probably incomplete. For example, they neglect the contribution to the NO^+ signal from the products of the reaction $CH_3SS + NO_2$, which probably takes place in their system, because it is very similar to ours. Similarly, CH_3SOH and S_2 are probably formed in their system, both of which could contribute to their signal at mass 64. The fragmentation of heavier species could also give ions at masses 30 or 64.

Tyndall and Ravishankara's[26] value was obtained by fitting the rise of NO to a biexponential form. These authors point out that the presence of vibrationally excited NO could affect their value. Also, they assumed that NO was formed only by the reactions of CH_3S and CH_3SO with NO_2. Although these authors have taken great care to minimize secondary chemistry, the presence of another source of NO would affect their determination. For example, CH_3S is not the only photolysis product of DMDS at the wavelength they used.[44] CH_3SS could also be formed and

(44) Suzuki, M.; Inoue, G.; Akimoto, H. *J. Chem. Phys.* **1984**, *81*, 5405.

TABLE II: Rate Constants for the Reactions of Sulfur Radicals with NO_2 at Room Temperature

reaction	rate const, cm^3 molecule^{-1} s^{-1}	ref
$S + NO_2 \rightarrow SO + NO$	6.5×10^{-11}	46
$HS + NO_2 \rightarrow HSO + NO$	6.7×10^{-11}	38
$CH_3S + NO_2 \rightarrow CH_3SO + NO$	5.1×10^{-11}	this work
$CH_3SS + NO_2 \rightarrow$ products	1.8×10^{-11}	this work
$SO + NO_2 \rightarrow SO_2 + NO$	1.4×10^{-11}	46
$HSO + NO_2 \rightarrow$ products	9.6×10^{-12}	43
$CH_3SO + NO_2 \rightarrow$ products	1.2×10^{-11}	this work
$CH_3SSO + NO_2 \rightarrow$ products	4.5×10^{-12}	this work

would give NO by reaction with NO_2.

The two rate constans k_1 and k_2 measured here support the trend reported by Lovejoy et al.[43] They noted that the rate constants of the R-S + NO_2 reactions are about 6×10^{-11} cm^3 molecule^{-1} s^{-1} and that those of the RSO + NO_2 reactions are about 1.2×10^{-11} cm^3 molecule^{-1} s^{-1}. Some relevant rate constant values are summarized in Table II. As one may have expected, the rate constants of the reaction of CH_3SS (k_3) and CH_3SSO (k_4) with NO_2 do not follow the rule, but it appears that the ratio k_3/k_4 follows the pattern observed for the other RS/RSO.

The atmospheric loss rates of CH_3S by oxidation by O_2, NO_2, and O_3 have already been discussed by Tyndall and Ravishankara.[26,46] They suggested that the reaction of CH_3S with O_3 yielded CH_3SO and that the subsequent reaction of CH_3SO with O_3 regenerated CH_3S in one or several steps and that therefore the reaction with O_3 would not result in a loss of CH_3S. Only an upper limit of 2.5×10^{-18} cm^3 molecule^{-1} s^{-1} is available for the rate constant of the $CH_3S + O_2$ reaction,[26] and this reaction could still be the main gas-phase loss of CH_3S in the atmosphere.

The present determination of k_2 allows the calculation of the atmospheric first-order rate constant of the reaction of CH_3SO with NO_2. In remote areas ($[NO_2] \approx 3 \times 10^8$ molecules cm^{-3}), the rate constant is about 4×10^{-3} s^{-1}, and in moderately polluted areas ($[NO_2] \approx 3 \times 10^{10}$ cm^{-3}), the rate constant is about 0.4 s^{-1}. Further studies of the reactions of CH_3SO with O_2 and O_3 are necessary to evaluate the atmospheric fate of CH_3SO.

Acknowledgment. This work was supported by NOAA as part of the National Acid Precipitation Assessment Program. Numerous stimulating and helpful discussions were held with E. R. Lovejoy over the course of this study.

(45) Clyne, M. A. A.; Whitefield, P. D. *J. Chem. Soc., Faraday Trans. 2* **1979**, *75*, 1327.

(46) DeMore, W. B.; Molina, M. J.; Sander, S. P.; Golden, D. M.; Hampson, R. F.; Kurylo, M. J.; Howard, C. J.; Ravishankara, A. R. *Chemical Kinetics and Photochemical Data for Use in Stratospheric Modeling, Evaluation No. 8*; Jet Propulsion Laboratory Publication 87-41, 1987.

(47) Tyndall, G. S.; Ravishankara, A. R. *J. Phys. Chem.* **1989**, *93*, 4707.

Kinetics of Sequential Energy-Transfer Processes

M. N. Berberan-Santos* and J. M. G. Martinho

Centro de Química-Física Molecular, Instituto Superior Técnico, 1096 Lisboa Codex, Portugal
(Received: November 21, 1989)

The kinetics of sequential excitation energy transfer in a four-species system have been studied and numerically exemplified for the case of a $t^{-1/2}$ dependence of the rate coefficients. It has been shown that previous treatments based on differential equations are incorrect owing to improper use of the rate coefficient derived for δ-pulse excitation.

Introduction

Sequential electronic energy transfer is an important process of frequency conversion and occurs in photosynthetic systems as a means to increase light collection performance. For instance, the wavelength-resolved fluorescence emission of the accessory pigments and chlorophyll *a* in the alga *Porphyridium cruentum* shows[1] that successive processes of energy transfer occur between the pigments until the electronic excitation energy reaches a reaction center, the pathway for 530-nm excitation being phycoerythrin to phycocyanin to allophycocyanin to chlorophyll *a* to reaction center. Recently, sequential energy transfer was also studied in Langmuir-Blodgett multilayers.[2]

The first kinetic model for the process of sequential transfer was that of Porter et al.[1] and consisted of a kinetic scheme of consecutive, irreversible transfers with rate coefficients having a $t^{-1/2}$ time dependence. These results were reproduced for other algae[3,4] and also used for Langmuir-Blodgett multilayers.[2] A major assumption leading to the $t^{-1/2}$ time dependence[5] is nevertheless not verified in these systems, namely the random distribution of acceptors in three dimensions.[6]

In this work, we present a more general treatment of the kinetics of irreversible sequential transfer (very weak coupling limit), numerically exemplified for the case of a $t^{-1/2}$ dependence of the rate coefficients.

The Kinetic Model

A general decay law for each of the species participating in the energy-transfer sequence can be written, for delta production, as

$$f_i(t) = \exp\left(-\frac{t}{\tau_i}\right) \exp\left(-\int_0^t k_{i\delta}(u)\, du\right) \qquad (1)$$

where τ_i is the intrinsic lifetime and $k_{i\delta}(t)$ the rate coefficient for energy transfer in step *i*. In the special case of a three-dimensional rigid solution of randomly distributed acceptors, it takes the form

(1) Porter, G.; Tredwell, C. J.; Searle, G. F. W.; Barber, J. *Biochim. Biophys. Acta* **1978**, *501*, 232-245.

(2) Yamazaki, I.; Tamai, N.; Yamazaki, T.; Murakami, A.; Mimuro, M.; Fujita, Y. *J. Phys. Chem.* **1988**, *92*, 5035-5044.

(3) Holzwarth, A. R.; Wendler, J.; Wehrmeyer, W. *Photochem. Photobiol.* **1982**, *36*, 479-487.

(4) Yamazaki, I.; Mimuro, M.; Murao, T.; Yamazaki, T.; Yoshihara, K.; Fujita, Y. *Photochem. Photobiol.* **1984**, *39*, 233-240.

(5) (a) Förster, T. *Z. Naturforsch.* **1949**, *4a*, 321. (b) Blumen, A.; Manz, J. *J. Chem. Phys.* **1979**, *71*, 4694.

(6) Hanzlik, C. A.; Hancock, L. E.; Knox, R. S.; Guard-Friar, D.; Maccoll, R. *J. Lumin.* **1985**, *34*, 99-106.

0022-3654/90/2094-5847$02.50/0